Reshaping Silica Particles: Mesoporous Nanodiscs for Bimodal Delivery and Improved Cellular Uptake

Valentina Giglio,[a,b] Silvia Varela-Aramburu,[c,d] Leana Travaglini,[b] Federica Fiorini,[b] Peter H. Seeberger,[c,d] Laura Maggini[b,*] and Luisa De Cola[b,e*]

a) Dipartimento di Scienze Chimiche, Università di Catania, Viale A. Doria 6, 95125 Catania, Italy.

b) Université de Strasbourg, CNRS, ISIS UMR 7006, F-67000 Strasbourg, France.

c) Max Planck Institute of Colloids and Interfaces, Department of Biomolecular Systems, Am Mühlenberg 1, 14476 Potsdam, Germany,

d) Freie Universität Berlin, Department of Biology, Chemistry, Pharmacy, Arnimallee 22, 14195 Berlin, Germany

e) Institut für Nanotechnologie (INT) - Building 640, Karlsruhe Institute of Technology (KIT) - Campus Nord, Hermann-von-Helmholtz-Platz 1, 76344 Eggenstein-Leopoldshafen, Germany

Email: lm690@cam.ac.uk, decola@unistra.fr

Keywords: Mesoporous silica nanoparticles • shape control • discoidal particles • drug delivery • monolayer

Acknowledgments

This work was financially supported by the European Research Council (ERC) Advanced Grant "MAGIC" (grant N° 247365), the Marie Skłodowska-Curie fellowship (MSCA-IEF) "POP-SILICA" (grant N° 627788) and the SACS Project (grant N° 310651), the Fondation ARC through the project "Thera-HCC" (grant N° IHU201301187), the Région Alsace, and the Département du Bas-Rhin. LDC especially acknowledges AXA Research funds. PHS and SVA acknowledge the Max Planck Society for generous funding. The authors thank Pengkun Chen for nitrogen adsorption and XPS measurements, Jeannette Steffen for ICP-AES measurements and Heike Runge for SEM assistance.

TOC

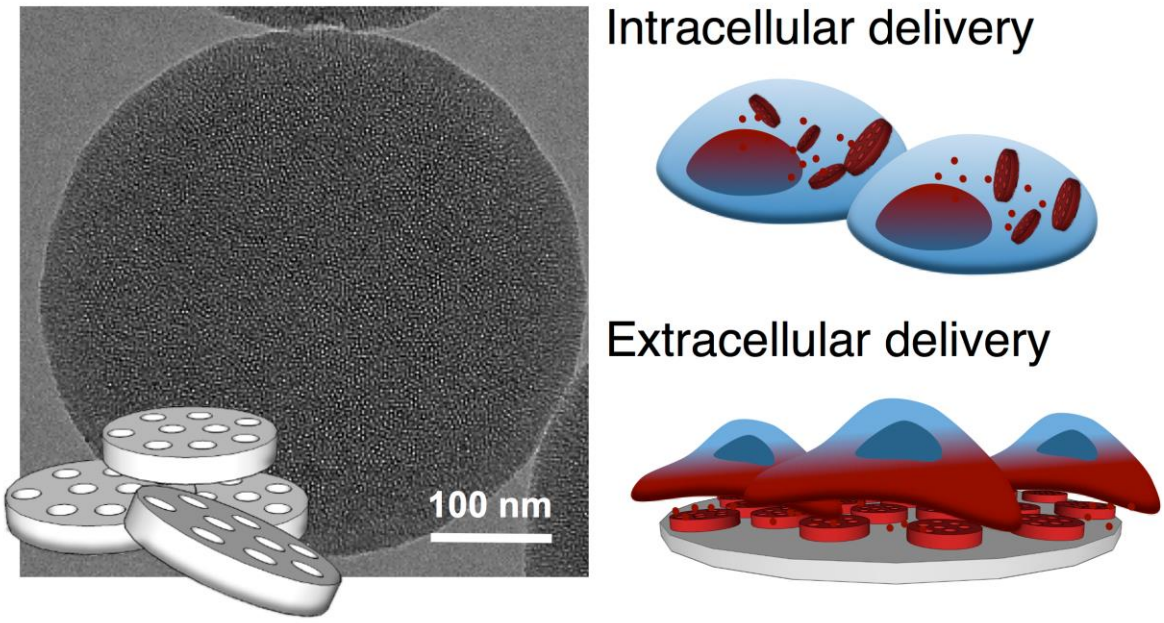

Bottom-up synthesis of flat, disc-shaped mesoporous silica nanoparticles, Nanodiscs (NDs), and their delivery applications are reported. The **NDs** can be readily internalized by cells or assembled in ordered monolayers, promptly releasing their payload both once internalized or in contact with cells adhering to their flat surface. The initial biological investigations underscore the potential these particles hold for intracellular and surface-mediated delivery applications, representing a significant addition to the biomedical MSNs toolbox.

Abstract: The role played by the shape of mesoporous silica nanoparticles has been investigated for intra- and extracellular delivery. Specifically, we have developed the bottom-up synthesis of flat disc-shaped mesoporous silica nanoparticles, the Nanodiscs (**NDs**). Due to their peculiar shape and large porous system, **NDs** present a higher cellular uptake than commonly investigated spherical mesoporous nanoparticles. Moreover, **NDs** are able to efficiently perform exhaustive delivery of their therapeutic cargo when loaded with the anticancer drug Doxorubicin and administered *in vitro* to cancerous HeLa cells. Thanks to their aspect ratio, **NDs** can also be readily assembled into well-organized monolayers to be employed in HeLa cells adhesion experiments upon preliminary functionalization with a specific targeting ligand. In these conditions **NDs** are able to deliver a hydrophobic dye to adhered cells *via* the highly accessible vertically aligned pores and their flat surface that ensures optimal cell contact. This initial investigation on the performance of **NDs** in both intra- and extracellular delivery activities suggests the great potential of these particles.

1. Introduction

Mesoporous silica nanoparticles (MSNs) hold great potential for theranostics applications because of their unique properties, such as hydrophilic surface favoring blood circulation, versatile silane chemistry for facile functionalization, biocompatibility, ease of large-scale synthesis and low production costs.[1,2] The physical parameters of MSNs have been tuned, as observations in biological systems suggest that factors like size, surface charge and shape, can vastly affect nonspecific uptake into cells, and furthermore potentially induce cellular responses.[3]

Particle shape is an important parameter, as it plays an important role in particle interactions with cells *in vitro*,[3-5] and in determining how particles navigate the bloodstream and distribute in tissues *in vivo*.[6-8] When shape is decoupled from volume, charge and material composition, mammalian epithelial cells preferentially internalize disc- or rod-shaped hydrogel particles, rather than spherical ones.[9] Disc-shaped porous silicon particles accumulate in tumors when injected *in vivo* because of a peculiar tendency to margination toward the blood vessel walls when circulating in the bloodstream.[10-11]

To date, mainly spherical (porous, hollow, multishell and rattle) and rod-shaped MSNs particles[3] have been evaluated for their cellular uptake since other morphologies are hard to prepare with sufficient control of dispersity. Mesoporous silica nanorods penetrate tumor tissues more rapidly than nanospheres, most likely because of improved transport through pores,[12] and those with larger aspect ratio (AR) are taken up by cells to a higher extent and with faster internalization rates.[13] Moreover, the AR of rod-shaped MSNs was also found to play a role on the activation of the micropinocytosis process in cancer cells.[14] The possibility to produce other MSN morphologies would lay the basis for gaining better insights into the effect of shape on their cellular uptake and drug delivery performance. For example, flat discoidal MSNs may be accepted better by certain cellular internalization pathways or possess enhanced EPR effect, as demonstrated for hydrogel and silicon disc-shaped particles. Moreover, a flat and homogeneous morphology may afford a length and orientation of pores that are beneficial for MSN in implants and surface-mediated drug delivery devices.

Here we report the bottom-up synthesis of the Nanodiscs (**NDs**), flat discoidal mesoporous silica nanoparticles, and an initial investigation of their biological applications. This novel material is internalized into HeLa cancer cells and performs better, in intracellular drug delivery, than 100 nm spherical MSNs (**MSN_{100}**). Furthermore, to challenge **NDs** in the delivery of their payload both intracellularly and extracellularly, these particles were also employed in the preparation of self-

assembled monolayers (SAMs) for targeted cancer cell adhesion and surface-mediated delivery experiments.[15-19]

2. Results and Discussion

2.1 Synthesis and characterization of NDs

The **NDs** were synthesized using a modified Stöber protocol, employing tetramethyl orthosilicate (TMOS) as silica source and octadecyltrimethylammonium chloride (OTACl) as template in a water/methanol 60/40 (w/w) mixture and in the presence of NaOH as catalyst (Fig. 1a; see SI, for complete synthetic details). Scanning and transmission electron microscopy (SEM and TEM; Fig. 1b-d; see also Fig. S1-2) of **NDs** displayed a homogenous flat discoidal morphology, characterized by an average diameter and thickness of 507.8 ± 93.8 nm and 80.0 ± 4.0 nm, respectively.

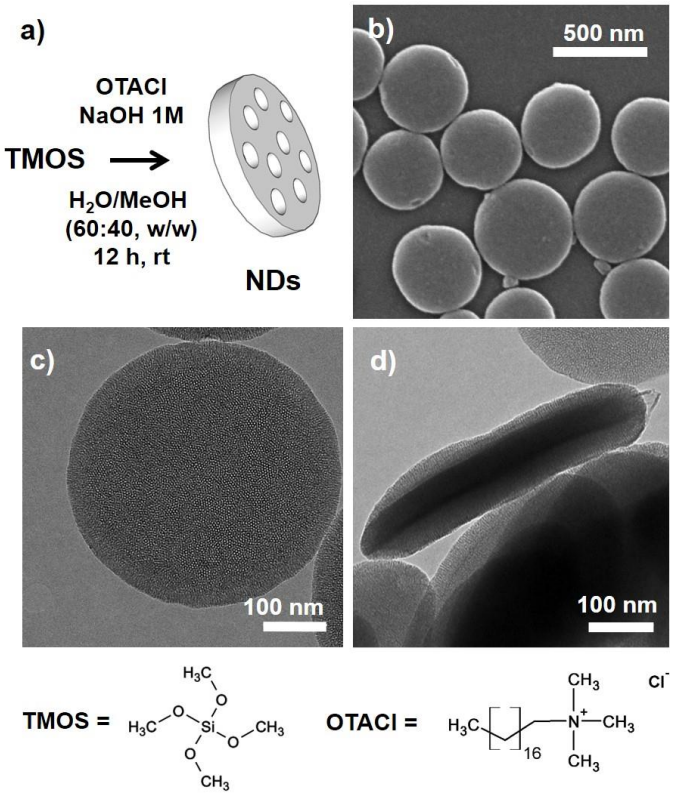

Figure 1: a) Schematic representation of the synthetic procedure for the synthesis of the **NDs**; b) SEM and c-d) TEM images of the **NDs**.

Under alkaline conditions and at the surfactant concentration used, the formation of the particles occurs through a cooperative self-assembly mechanism, as reported in the literature.[20-22] *In situ* measurements on similar systems suggest in fact that in the initial phase of the process silicate anions interact electrostatically with spherical surfactant micelles, leading to the formation of silica-surfactant aggregates that grow and assemble as silica polymerization occurs. The resulting composite mesostructured material eventually precipitates out of the reaction mixture.[20]

It is well known that the synthesis of mesoporous silica is a process extremely sensitive to the experimental conditions used and to the specific chemistry and interactions involved in each investigated system. The slightest modification of these parameters can lead to the variation of size, shape and porosity of the produced particles. It follows that the explanation of the formation of the discoidal **NDs** resides in the reported experimental conditions. Exploratory experiments were thus carried out in order to assess the influence of several parameters on the synthesis of **NDs** (Fig. S3). It resulted that the H_2O content of the solvent mixture influences significantly the morphology of the produced particles.[23,24] By gradually decreasing the water content in the H_2O/MeOH mixed solvent from 60/40 to 30/70 (w/w) we observed a gradual shift of the morphology of the product from discoidal to spherical (Fig. S3a-d). Specifically, when decreasing the water content to 50/50 (w/w) we seem to loose some control on the morphology of the product obtaining irregular thinner, wider discs compared to the **NDs** (Fig. S3c). By further decreasing the water content of the mixed solvent we obtain first polydisperse and then larger regular spherical particles at 40/60 and 30/70 (w/w) percentages respectively (Fig. S3a-b). The water content is evidently playing an important role in molding the morphology of the **NDs**, with a higher water fraction of the mixed solvent favoring the formation of discoidal particles over spherical ones.

This central role may be explained by the fact that the water content affects directly: (i) the self-assembly of the surfactant; and (ii) the hydrolysis of the silane. Undeniably, a higher content of water induces a decrease of the surfactant critical micellar concentration and increase of aggregation number (the number of molecules present in a micelle),[25,26] as well as affecting the composition of the solvation shell.[26] This is because as the concentration of MeOH decreases the alcohol molecules in the solvation cell are replaced by H_2O, partially screening the headgroups of the surfactant thus promoting the micellar aggregation process. The solubility of the silane, TMOS (soluble in organic solvents), is negatively affected by the addition of water to the reaction mixture. Yet, at the same time water enhances its hydrolysis rate, prompting a faster condensation of silica. These considerations suggest that the discoidal shape of **NDs** is therefore achieved in experimental conditions where a fast condensation of silica occurs on very compact micelles, which form at lower concentration and aggregate easily.[27]

To confirm the importance of the kinetics of condensation of silica in the formation of the **NDs**, we performed a test reaction by lowering the pH of the reaction mixture, another important parameter affecting the hydrolysis of the silane. At pH ≈ 10 (≈ 12 for the standard **NDs** synthetic conditions; Fig. S3e) the particles obtained are again less regular, inhomogeneous, brittle discoidal particles compared to **NDs**, characterized by a lower degree of condensation.

The preparation of **NDs** is also very specific for the surfactant employed. Variations in the counterion and the length of the aliphatic chain lead to different packing geometries and interactions with the silicates, resulting in very different products. For example, when we attempted the synthesis of the **NDs** by replacing the surfactant OTACl with cetyltrimethylammonium bromide (CTAB), spherical particles were obtained (Fig. S3f). Since at the used concentration (11.5 mM) both the surfactants are expected to form spherical micelles before the addition of TMOS, even though slightly bigger for the OTACl, the major role in the formation of discoidal particles may be attributed to the counterion that influences the interactions between the micelles and the growing silicates. Depending on its binding efficiency, the counterion blocks the adsorption of silicate ions onto the micellar surface during the condensation process, and it is known that the binding efficiency follows the Hofmeister series, according to which Cl^- is one of the least binding.[28-29] It follows that Cl^-, being the least bound to the micelles most likely favors the occurrence of the attractive electrostatic forces between the polysilicates and the surfactant micelles and therefore determines a faster growth of the composite material, leading to formation of the **NDs**, the kinetically favored products as supported also by the above mentioned experiments.

Comprehensive morphological and physicochemical analyses of the **NDs** were performed to fully characterize the particles. SEM and TEM imaging of the **NDs** (Fig. 1b-d) evidenced the consistent discoidal morphology of the material. TEM on calcined **NDs** also revealed the presence of a porous framework in the particles. N_2 adsorption analysis of the **NDs** measured a BET surface area of 863 m^2/g, total pore volume of 0.83 cm^3/g, and an average pore diameter value of 3.8 nm (Fig. S4). Further confirmation of the porous structure was provided by the small-angle X-ray scattering (SAXS) pattern that presented two broad signals, centered at q = 1.7 and 3.2 nm^{-1} (Fig. S5), consistent with the (100) and (110) planes of hexagonal mesostructures. Even though the broad peaks suggest the absence of a long range ordering of pores, the value of the d_{100} spacing = 3.7 nm is in agreement with the pore diameter distribution determined by N_2 adsorption analysis. Elemental composition of **NDs** was determined by X-ray photoelectron spectroscopy (XPS; Fig. S6a, and Table S1). The particles, as expected, were found to be mainly composed of Si(2p) (28.1 ± 0.7 atomic percentage [At%]) and O(1s) (63.6 ± 0.3 At%). Thermogravimetric analysis (TGA) only exhibited a negligible weight loss (3.1%, Fig. S7) in the investigated temperature range (100-750 °C), attributable to the condensation of silanol groups. Finally, the recorded ζ-potential of **NDs**, -25.9 ± 1.2 mV, in PBS (pH 7.4) confirmed the negative surface charge for these silica nanoparticles in physiological conditions (Fig. S8).

2.2 Biocompatibility, cellular uptake and biodegradation of NDs

Once the **NDs** have been characterized, the investigation of the cellular uptake, cytotoxicity, and drug delivery of these particles was tackled as a first evaluation of their possible use for biomedical applications. HeLa cells were initially incubated with **NDs** at two different concentrations, 50 and 100 µg/mL (Fig. S9), and the viability was evaluated after 3, 24 and 72 hour incubation. Negligible cell death was detected indicating very low cytotoxicity of the **NDs** in the concentration range tested.

The cellular association of **NDs** was quantified by using flow cytometry analysis (FACS). The particles were labeled with Rhodamine B through a post-synthetic grafting (**r-NDs**, see SI for details; Fig. S10) and incubated with HeLa cells at a concentration of 50 and 100 µg/mL, for 3, 24 and 72 hours. To assess the effect of the discoidal shape on the cellular uptake of MSNs we compared **r-NDs** to Rhodamine B-labeled 100 nm spherical MSNs (**r-MSN$_{100}$**, see SI; Fig. S10), possessing the same surface charge (Fig. S8). Interestingly, for both the employed concentrations the FACS measurements after 3 hours indicated a more efficient association of **r-NDs** to the cancerous cells compared to the **r-MSN$_{100}$** (FACS; Fig. 2a for 50 and S11 for 100 µg/mL). After 24 and 72 hours of incubation the percentage of positive cells further increased for **r-NDs**, as up to 50% of the cell population resulted positively tagged. In contrast, for **r-MSN$_{100}$** the association decreased in time becoming negligible after 72 hours.

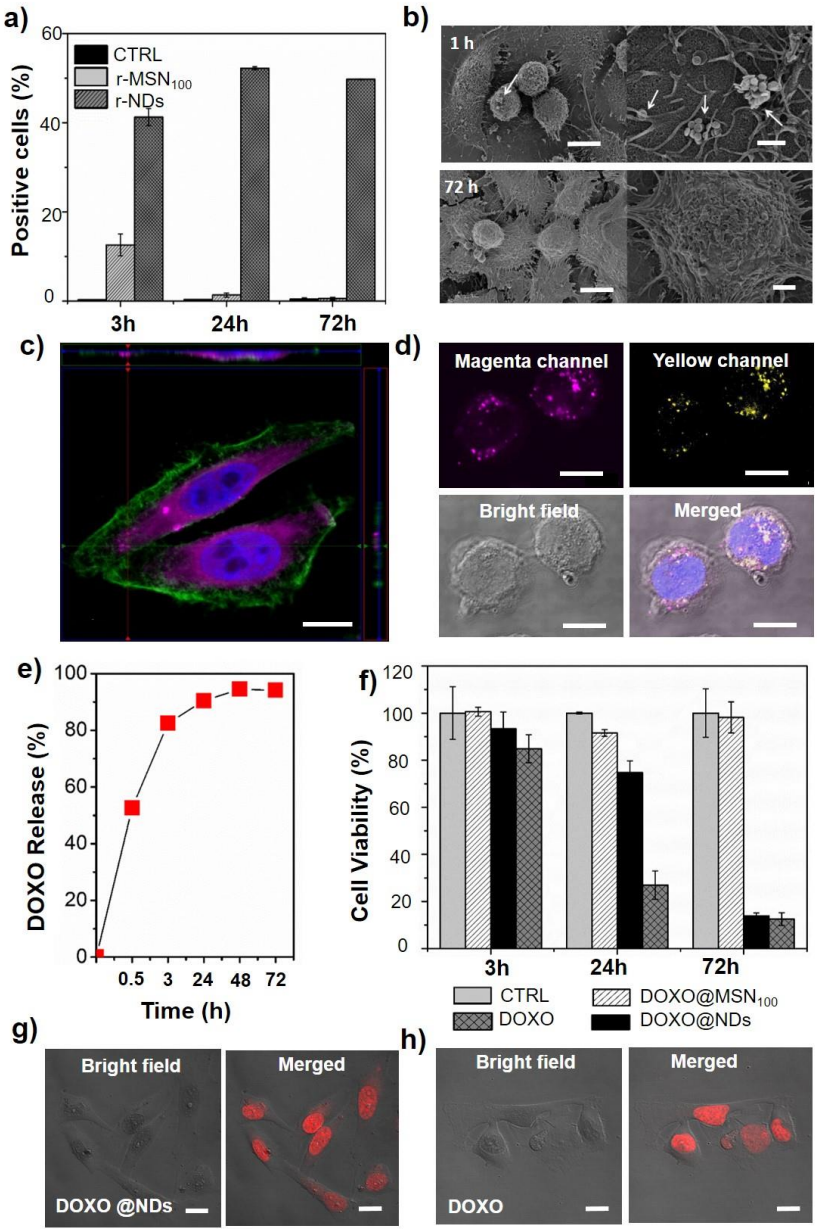

Figure 2: a) FACS analysis of the cellular uptake of **r-NDs** (50 µg/mL) in HeLa cells upon 3, 24 and 72 h incubation. **r-MSN$_{100}$** were tested for comparison; b) SEM images of HeLa cells incubated with **r-NDs** at a concentration of 50 µg/mL for 3 h, further washed and incubated with fresh medium for 1 h. Scale bar = 10 µM (sx) and 1 µM (dx); c) Z-stack confocal imaging of the **r-NDs** after 3 h incubation in HeLa cells. Magenta channel = Rho; green channel = Phalloidin Alexa Fluor® 647; blue channel = DAPI. Scale bar = 10 µM; d) Confocal images of **r-NDs** after 1 h incubation in Hela cells for co-localization experiment. Magenta channel = Rho; Yellow channel = LysoTracker®. Scale bar = 10 µM; e) DOXO release profile from **DOXO@NDs** in PBS (pH 7.4; conc. = 0.1 mg/mL); f) cytotoxicity of **DOXO@NDs** when incubated in HeLa at 50 µg/mL for 3, 24 and 72 h. **DOXO@MSN$_{100}$** and DOXO alone were also tested as reference, keeping either the dose or the content of DOXO constant; g,h) confocal images of the uptake of **DOXO@NDs** and DOXO after 3 h incubation. Red channel = DOXO. Scale bar = 10 µM.

To understand whether the **r-NDs** detected by FACS were only externally bound or rather endocytosed by the cancerous cells and define the evolution in time of their localization, we

performed SEM investigations and confocal laser scanning microscopy (CLSM) of HeLa cells exposed to **r-NDs**. Specifically, HeLa cells were incubated for 3 hours at 50 µg/mL before washing and addition of fresh culture medium (CM). The cells were then further incubated for 1, 24 and 72 hours to perform SEM and CLSM analysis.

SEM imaging of the surface of cancer cells (Fig. 2b; see also Fig. S12) showed that 1 hour after incubation and CM renewal, few **r-NDs** clusters are detected on the cell surface. No loose **r-NDs** aggregates could be detected in the sample. Interestingly, after 24 and 72 hours (Fig. S12), the externally bound **NDs** could no longer be imaged most probably as a result of a slow uptake process, as reported for larger silicon discoidal particles.[30]

Internalization of **r-NDs** was confirmed by CLSM. The Z-stack images (Fig. 2c; see also Fig. S13) of HeLa cells after 3 hours incubation at 50 µg/mL, recorded after membrane staining with Phalloidin Alexa Fluor® 647, clearly demonstrated the presence of **r-NDs** inside the cancerous cells. The subcellular localization of the internalized particles was further investigated by employing the lysosome-specific fluorescent marker Lysotracker® Deep-Red (Fig. 2d; see also Fig. S14). To obtain an objective evaluation of the labeled vesicles, the fluorescent signals of the **r-NDs** and the stained organelles were quantified using ImageJ software. After 1 hour, 65% of Lysotracker-positive vesicles were also labeled with **r-NDs** (Pearson's correlation coefficient: 0.652). This indicates that the nanoparticles are internalized *via* classical endocytosis, as observed for both large silicon discoidal particles[30] and **MSN$_{100}$**.[31] In agreement with the trend detected by FACS, after 24 hours the co-localization increased to 74% (Pearson's correlation coefficient: 0.743; Fig. S14), probably due to further internalization of the aggregates present on the cell surface. After 72 hours, the co-localization decreased to 53% (Pearson's correlation coefficient: 0.534; Fig. S14). This drift, not related to the lesser association reduction detected by FACS, could either reflect a loss of signal from Lysotracker or the partial degradation and escape of the particle debris from the lysosomes.

To confirm the latter hypothesis we investigated the stability of **NDs** in HeLa cells by measuring the concentration of the silicon in the incubation medium by means of inductively coupled plasma atomic emission spectrometry (ICP-AES).[32] We performed this analysis because once the internalized nanoparticles start to degrade, small silica debris are released in the CM, in which no other form of Si is present. Again, HeLa cells were incubated for 3 hours at 50 µg/mL before washing, addition of fresh CM and further incubation for 1, 24 and 72 hours, at which time points ICP-AES analysis was performed. From the data reported in Table 1 it is clear that Si was only detected in the CM of the cancer cells incubated with **NDs** and not in the CM of cells not

incubated with particles used as control. Moreover Si concentration resulted increasing with time, in line with the assumption that there is a constant degradation of the internalized particles. In similar experimental conditions **MSN$_{100}$** did not present any sign of degradation,[31] possibly indicating an influence of the aspect ratio and the highly ordered mesostructure of **NDs** on their degradation. Yet, these preliminary studies do not address such correlation and more investigation will be undertaken to elucidate this interesting aspect.

Table 1. ICP-AES results for the detection of Si in the CM of HeLa cells and HeLa cells previously incubated with **NDs** at 50 µg/mL for 3 h and washed.

	Si / ppm	
	NDs	Control
1 h	0.15 ± 0.05	--
24 h	1.09 ± 0.02	--
72 h	1.70 ± 0.10	--

2.3 Drug delivery performance of NDs

After establishing that the **NDs** are biocompatible and efficiently taken up by cancer cells, we investigated their activity as drug delivery system. **NDs** were loaded with the anticancer drug Doxorubicin (DOXO; **DOXO@NDs**, see SI), and the loading established by means of UV-Vis spectroscopy (25wt.%, Fig. S15). The release kinetics of the drug from **DOXO@NDs** in PBS (pH 7.4) was first evaluated spectroscopically over a 72 hours timespan (Fig. 2e). The drug release process is characterized by a burst discharge occurring immediately after incubating the **DOXO@NDs** in PBS, possibly due to superficially adsorbed DOXO molecules and molecules close to the channel entrance, followed by a sustained release over the rest of the measurement, until complete unloading of the drug. Since the **NDs** mostly preserved their structural integrity in PBS (pH 7.4) when stirred at 37 ˚C up to 7 days (Fig. S16), the release kinetics should be attributed mainly to the escape of the drug molecules from the porous structure. Indeed, only partial exfoliation and few cracks were detected for **NDs** under these conditions, as the degradation of MSNs is known to decelerate with the size, and most importantly the aspect ratio of the particle.[33]

HeLa cells were treated with 50 and 100 µg/mL of **DOXO@NDs** (corresponding to a DOXO content of 12.5 and 25 µg/mL; Fig. 2f and S17 for the treatment of HeLa cells with 50 and 100 µg/mL respectively). After 3, 24 and 72 hour incubation, the cells were washed with PBS and their viability measured. Free DOXO, **NDs**, **MSN$_{100}$** in their pristine form and loaded with DOXO (**DOXO@MSN$_{100}$**; see SI), all containing the same content of DOXO, were also incubated for

comparative purpose. Both **NDs** and **MSN$_{100}$** did not show significant cytotoxicity at the concentrations tested at any of the time points. Similarly to free DOXO, after 3 hours of incubation HeLa cells treated with **DOXO@NDs** suffered a viability decrease to about 90-80% for 50 and 100 µg/mL respectively. Confocal images recorded after 3 hours incubation of **DOXO@NDs** in HeLa cells at 50 µg/mL (Fig. 2g) already displayed a high concentration of the anticancer drug in the nuclei, confirming the easy escape of the drug from the porous framework. Small aggregates present on the surface of the cells, and ready to be internalized, are also detected. After 24 and 72 hours of incubation of **DOXO@NDs** the cell viability further dropped to 70-50% and after 72 hours it dropped to 10%, with an overall cytotoxic effect comparable to that of the free anticancer drug. These data not only indicate that **NDs** grant exhaustive release of their payload, but also confirm the very efficient cellular uptake of these particles, as well as their complete biocompatibility. On the contrary, **DOXO@MSN$_{100}$** only presented minor cytotoxicity after 3 hours incubation, whilst after 24 and 72 hours the viability of HeLa cells only decreased to 70-80%, the drug payload being equal.

The therapeutic activity **DOXO@NDs** likely derives from a synergistic effect of their efficient cellular uptake and their efficiency in releasing the drug from their porous framework. **NDs** preserve the loaded DOXO from degradation and dispersion in the CM and, due to their high affinity for the cells, convey all their cargo within the cellular environment where it is free to perform its therapeutic activity. Since chemotherapeutic drugs have adverse side effects, drug loading in a non-cytotoxic nanocarrier for controlled release is preferred for *in vivo* applications. **NDs**, granting complete cellular uptake and a gradual yet exhaustive intracellular drug release, would confine the cytotoxic activity of the drug thus mitigating its side effects and allowing less frequent administrations.

2.4 Surface-mediated delivery from NDs monolayers

The advantage of the disc-shaped morphology on the implementation of MSNs based devices was demonstrated by preparing a dye-releasing SAM of **NDs** for cell adhesion experiments and *in situ* staining of the adsorbed live cells (Fig. 3a). Specifically, **NDs** were loaded with Nile Red (NR; **NR@NDs**, see SI), a hydrophobic dye able to stain the membrane of cells,[34] and the particle surface functionalized with (3-aminopropyl)triethoxysilane (APTES; **NR@NDs-APTES**, see SI), to allow for grafting onto a pre-activated glass substrate (see SI).[35] Nile red encapsulation, as well as the grafting of the amino-silane on the **NR@NDs**, were monitored by means of XPS and TGA analysis (Fig. S6b-c, and Table S1). The covalent binding of APTES on the surface, **NR@NDs-APTES**, was further confirmed by a strong shift of ζ-potential in solution, from the negative

unfunctionalized silica to a positive value of the protonated amines (+19.6 ± 0.5 mV; Fig. S8). Fluorescence spectroscopy confirmed the presence of the dye in both hybrids (Fig. S18).

The SAMs were prepared following a procedure previously reported for zeolites.[35] SEM images of the monolayers of **NDs** (Fig. 3b, Fig. S19) highlighted a homogenous particle distribution, without significant vertical stacking or tilting of the particles, providing a large flat contact area for the adhesion of the cancerous cells. Confocal analysis confirmed persistence of NR within the SAMs (Fig. S20) when the monolayers were immersed in water based solutions. To favor adhesion of the cancerous cell line, the surface of the monolayer was functionalized with folic acid (FA), a HeLa cells specific targeting moiety (**FA-SAM**, see SI).[36] The bio-coating was confirmed by high resolution XPS analysis, which shows the N(1s) and C(1s) signals of **FA-SAM**, at the energy characteristic for amidic bonds between the anchored aminopropylsilane and the FA (Fig. S21).[37]

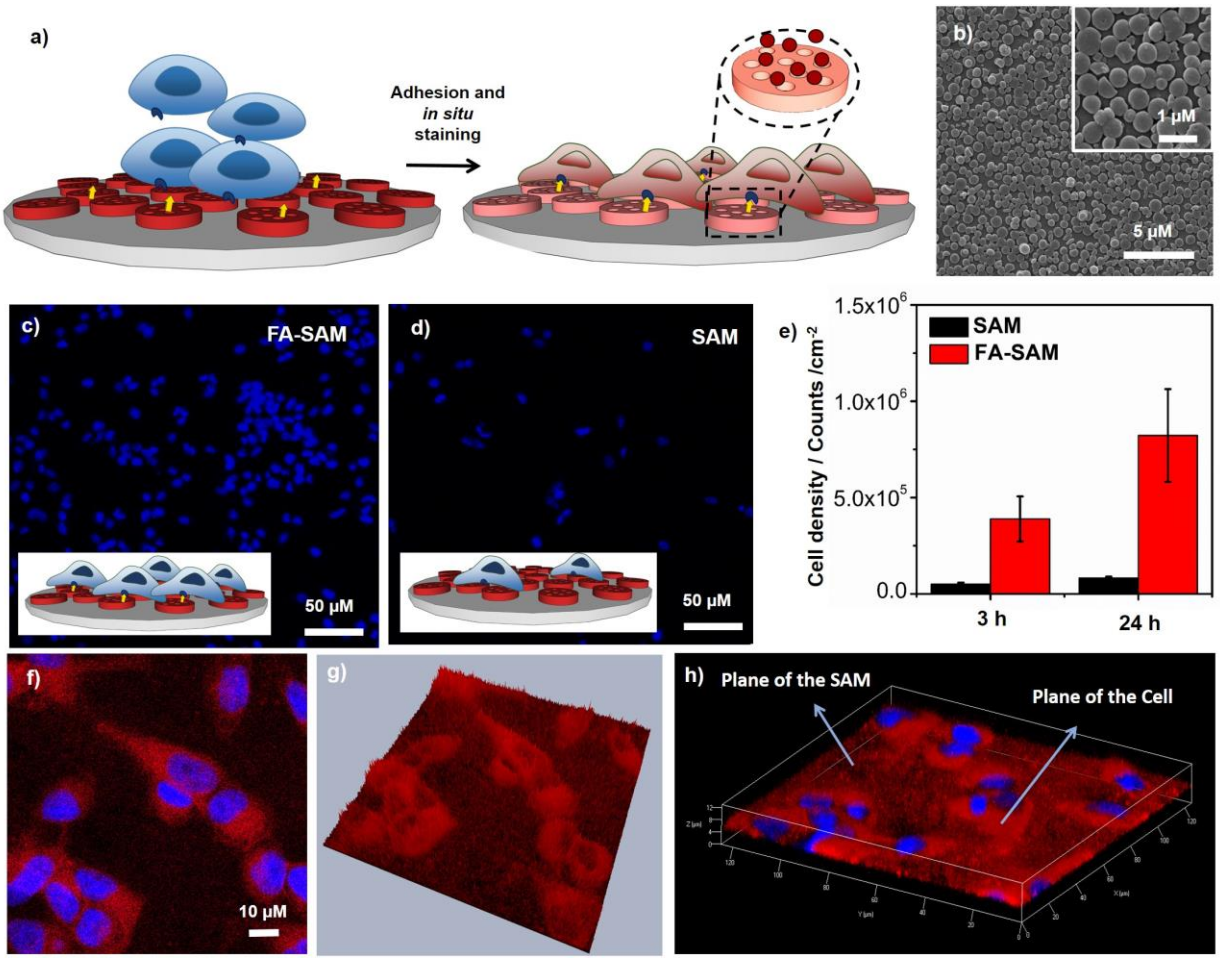

Figure 3: a) Graphical representation of the *in situ* cellular staining experiment; b) SEM image of the **FA-SAM** of **NDs**. In the inset an enlarged image of the monolayer; c-d) confocal images of HeLa cells adsorbed on **FA-SAM** and SAM, respectively (blue channel = DAPI); e) cell counting of the HeLa cells adsorbed onto the monolayers; f-h) confocal 2D,

2.5 and 3D images of the HeLa cells adsorbed onto **FA-SAM**, after 24 h adhesion, fixation and staining with DAPI. Red channel = NR, blue channel = DAPI.

With the morphology and the surface functionalization of the SAMs confirmed, adhesion experiments were carried out. Control SAMs, without the targeting units, were also prepared and used as control. HeLa cells were seeded on **FA-SAM** and, after 3 and 24 hours of incubation at 37 °C, the cells were fixed with paraformaldehyde (4 wt.% in PBS) and the nuclei stained with DAPI, to allow imaging and counting of the cells at the confocal microscope. As shown in Figures 3c-d (see also Fig. S22), the adhesion of cancer cells on the monolayer was increased by the presence of FA (7.6 and 10-fold increase for the **FA-SAM** vs the control, after 3 and 24 hours of incubation, respectively; Fig. 3e). Analysis of the NR signal in the **FA-SAM** sample fixed after 24 hours of adhesion confirmed the presence of the dye homogeneously staining the adhered cells, endorsing the effective transfer of NR from the substrate to the cells (Fig. 3f-h). As mentioned the NR dye cannot escape the pores of the **NDs** because of its hydrophobicity (no NR release detected in the CM, Fig. S23). Therefore the efficient transfer of NR to the cells must be favored by the large flat surface area of the **NDs**, able to maximize the contact with the hydrophobic cell membrane of the cells, which provides a suitable environment for the spontaneous diffusion of the NR out of the monolayer

Another important factor enhancing the release activity of this monolayer is the consistent directional alignment of the pores of the discs, all perpendicularly oriented in respect to the adsorbed cells (not possible for spherical MSNs), allowing for complete exploitation of the loaded dye. The release was further monitored over time by live cell confocal microscope imaging (Fig. S24). This analysis demonstrated that the diffusion of the dye into the adsorbed cell layer starts shortly after the cells adhere, as the NR was already staining the HeLa within the first 3 hours of the experiment. The intensity of the emission of the NR in the cells increased with time, indicating a continuous diffusion of the dye and an efficient extracellular delivery of the hydrophobic molecules.

3. Conclusions

Flat disc-shaped mesoporous silica nanoparticle, obtained *via* a templated modified Stöber condensation process, have been synthesized and fully characterized, widening the range of morphologies of MSNs available for the preparation of tailored nanotheranostic agents. The **NDs** resulted able to efficiently deliver their cargo both intracellularly, when internalized in cancerous cells, and extracellularly, when part of bioactive surface-mediated drug delivery systems. The morphology of these particles boosted cellular uptake, and resulted exceptionally beneficial for fostering intimate and effective contact with the cells adsorbed onto the monolayers. In both the

intracellular and extracellular delivery application, the width and orientation of the pores of **NDs** maximized the externalization of the payload. Studies aimed at progressing the knowledge on the bioactivity of **NDs** once internalized in the cells and their biodistribution when injected *in vivo*, as well as the design of implantable devices containing the **NDs**, are currently on going and will further define the potential of these original mesoporous silica nanoparticles for nanotheranostic applications.

Supporting Information

Supplementary information (SI) available: full experimental procedures, additional SEM and TEM images of particles, size distribution, SAXS, N_2 adsorption, XPS, TGA, ζ-potential, photophysical measurements, confocal microscope images, FACS and cytotoxicity assays.

Bibliography

[1] Y. Wang, Q. Zhao, N. Han, L. Bai, J. Li, J. Liu, E. Che, L. Hu, Q. Zhang, T. Jiang, S. Wang, *Nanomedicine: NBM* **2015**, *11*, 313-327.

[2] Q. He, J. Shi, *Adv. Mater*. **2014**, *26*, 391-411; c) M. Colilla, B. González a, M. Vallet-Regí, *Biomater. Sci*. **2013**, *1*, 114-134.

[3] N. Hao, L. Li, F. Tang, *J. Biomed. Nanotechnol.* **2014**, *10*, 2508-2538.

[4] S. E. A. Gratton, P. A. Ropp, P. D. Pohlhaus, J. C. Luft, V. J. Madden, M. E. Napier, J. M. De Simone, *Proc. Natl. Acad. Sci. USA* **2008**, *105*, 11613-11618.

[5] J. A. Champion, Y. K. Katare, S. Mitragotri, *J. Control. Release* **2007**, *121*, 3-9.

[6] R. Toy, P. M. Peiris, K. B. Ghaghada, E. Karathanasis, *Nanomedicine* **2014**, *9*, 121-134.

[7] T.-R. Lee, M. Choi, A. M. Kopacz, S.-H. Yun, W. K. Liu, P. Decuzzi, *Sci. Rep*. **2013**, *3*, 2079.

[8] P. Decuzzi, B. Godin, T. Tanaka, S. Y. Lee, C. Chiappini, X. Liu, M. Ferrari, *J. Control. Release* **2010**, *141*, 320-327.

[9] R. Agarwal, V. Singh, P. Jurney, L. Shi, S. V. Sreenivasan, K. Roy, *Proc. Natl. Acad. Sci. USA* **2013**, *110*, 17247- 17252.

[10] B. Godin, C. Chiappini, S. Srinivasan, J. F. Alexander, K. Yokoi, M. Ferrari, P. Decuzzi, X. Liu, *Adv. Funct. Mater*. **2012**, *22*, 4225-4235.

[11] E. Tasciotti, X. Liu, R. Bhavane, K. Plant, A. D. Leonard, B. K. Price, M. M.-C. Cheng, P. Decuzzi, J. M. Tour, F. Robertson, M. Ferrari, *Nat. Nanotechnol*. **2008**, *3*, 151-157.

[12] V. P. Chauhan, Z. Popović, O. Chen, J. Cui, D. Fukumura, M. G. Bawendi, R. K. Jain, *Angew. Chem. Int. Ed.* **2011**, *50*, 11417-11420.

[13] X. L. Huang, X. Teng, D. Chen, F. Q. Tang, J. Q. He, *Biomaterials* **2010**, *31*, 438-448.

[14] H. Meng, S. Yang, Z. Li, T. Xia, J. Chen, Z. Ji, H. Zhang, X. Wang, S. Lin, C. Huang, Z. Hong Zhou, J. I. Zink, A. E. Nel, *ACS Nano* **2011**, *5*, 4434-4447.

[15] D. Böcking, O. Wiltschka, J. Niinimaki, H. Shokry, R. Brenner, M. Linden, C. Sahlgren, *Nanoscale* **2014**, *6*, 1490-1498.

[16] N. S. Kehr, H.-J. Galla, K. Riehemann, H. Fuchs, *RSC Adv.* **2015**, *5*, 5704-5710.

[17] B. Ergün, L. De Cola, H.-J. Galla, N. S. Kehr, *Adv. Healthcare Mater*. **2016**, *5*, 1588-1592.

[18] C. Chiappini, J. O. Martinez, E. De Rosa, C. S. Almeida, E. Tasciotti, M. M. Stevens, *ACS Nano* **2015**, *9*, 5500–5509.

[19] N. S. Kehr, A. Motealleh, A. H. Schäfer, *ACS Appl. Mater. Interfaces* **2016**, *8*, 35081–35090.

[20] K. J. Edler, *Aust. J. Chem*. **2005**, *58*, 627– 643.

[21] J. Patarin, B. Lebeau, R. Zana, *Curr. Opin. Colloid Interface Sci.* **2002**, *7*, 107–115.

[22] Y. Wan, D. Zhao, *Chem. Rev*. **2007**, *107*, 2821–2860.

[23] C. A. Milea, C. Bogatu, A. Duta, *Bull. Trans. Univer. Braşov Ser I*: *Eng. Sci*. *4*, 59–66.

[24] M. T. Anderson, J. E. Martin, J. G. Odinek, P. P. Newcomer, *Chem. Mater*. **1998**, *10*, 1490-1500.

[25] J.-B. Huang, M. Mao, B.-Y. Zhu, *Colloids Surf. A Physicochem. Eng. Asp.***1999**, *155*, 339–348.

[26] W. Li, Y.-C. Han, J.-L. Zhang, B.-G. Wang, *Colloid J*. **2005**, *67*, 159–163.

[27] H.-P. Lin, C.-P. Kao, C.-Y. Mou, *Microporous and Mesoporous Mater*. **2001**, *48*, 135–141.

[28] F. Hofmeister, *Arch. Exp. Pathol. Pharmakol.* **1888**, *24*, 247–260.

[29] E. Leontidis, *Curr Opin Colloid Interface Sci.* **2002**, *7*, 81–91.

[30] R. Xu, G. Zhang, J. Mai, X. Deng, V. Segura-Ibarra, S. Wu, J.Shen, H. Liu, Z. Hu, L. Chen, Y. Huang, E. Koay, Y. Huang, J. Liu, J. E Ensor, E. Blanco, X. Liu, M. Ferrari, H. Shen, *Nat. Biotechnol.* **2016**, *34*, 414–418.

[31] L. Maggini, I. Cabrera, A. Ruiz-Carretero, E. A. Prasetyanto, E. Robinet, L. De Cola, *Nanoscale* **2016**, *8*, 7240–7247.

[32] I. Stayton, J. Winiarz, K. Shannon, Y. Ma, *Anal. Bioanal. Chem*. **2009**, *394*, 1595–1608.

[33] J. G. Croissant, Y. Fatieiev, N. M. Khashab, *Adv. Mat.* **2017**, *29*, 1604634–1604685.

[34] P. Greenspan, S. D. Fowler, *J. Lipid Res*. **1985**, *26*, 781-789.

[35] A. Greco, L. Maggini, L. De Cola, R. De Marco, L. Gentilucci, *Bioconjugate Chem.* **2015**, *26*, 1873–1878.

[36] C. Sun, R. Sze, M, Zhang, *J. Biomed. Mater. Res. Part A* **2006**, *78A*, 550–557.

[37] O. Olivares, N. V. Likhanova, B. Gomez, J. Navarrete, M. E. Llanos-Serrano, E. Arce, J. M. Hallen, *Appl. Surf. Sci.* **2006**, *252*, 2894–2909.